J Mol Model (2014) 20:2519
DOI 10.1007/s00894-014-2519-7

ORIGINAL PAPER

Theoretical study on the reaction mechanism of chlordimeform with OH radicals

Shengmin Sun · Kun Zhang · Yang Lu · Hui Zhang

Received: 30 June 2014 / Accepted: 3 November 2014 / Published online: 20 November 2014

Abstract A theoretical investigation on the multiple-channel degradation mechanism of chlordimeform with OH radicals in the atmosphere was completed using a dual-level direct dynamics method. The equilibrium geometries and the corresponding harmonic vibrational frequencies of the stationary points were obtained at the M06-2X/6-311++G(d,p) level. The minimum energy paths (MEP) were calculated at the same level, and energetic information was further refined at M06-2X/6-311++G(3df,2p) level. The rate constants for the 15 reaction channels were calculated by improved canonical variational transition state theory with small-curvature tunneling correction over the temperature range 200–1,000 K. The total rate constants are in good agreement with the available experimental data and the three-parameter expression $k(T) = 2.62 \times 10^{-18} T^{2.71} \exp(899.61/T)$ $cm^3 molecule^{-1} s^{-1}$ was given. The calculated results indicate that the addition reaction of the carbon–nitrogen double bond is the major channel, while the abstraction reaction from the benzene ring of chlordimeform is the least competitive channel.

Keywords Gas-phase reaction · Rate constant · Transition state · Chlordimeform

Electronic supplementary material The online version of this article (doi:10.1007/s00894-014-2519-7) contains supplementary material, which is available to authorized users.

S. Sun · K. Zhang · Y. Lu · H. Zhang (✉)
College of Chemical and Environmental Engineering, Harbin University of Science and Technology, Harbin 150080, People's Republic of China
e-mail: hust_zhanghui11@hotmail.com

S. Sun
College of Food Engineering, Harbin University of Commerce, Harbin 150076, People's Republic of China

Introduction

Chlordimeform is a type of broad spectrum acaricide that has insecticidal activity, killing the eggs of mites, ticks and some lepidopteran insects. The use of chlordimeform leads to its emission into the atmosphere by spray, volatilization and wind erosion. The misuse and overuse of pesticides can result in many problems, for example, excessive residues in honey can affect the health of consumers [1–8], chlordimeform can damage human cardiovascular function [9–11], and long-term exposure to chlordimeform can significantly increase the incidence of bladder cancer [12–16]. Chlordimeform has been listed in *Priority Pollutants* prescribed by China. The degradation mechanisms of chlordimeform have attracted research interest [17–21]. The chemical conversions of chlordimeform in the atmosphere are mainly the reactions with oxidants (such as hydroxyl, O_3, and NO_3) and photolysis. The reaction of chlordimeform with OH radical is the most important reaction [22–24], consisting of several reaction channels, including possible reaction channels initiated by hydroxyl on the side-chain and the benzene ring. A total of 15 possible reaction channels have been identified for the reaction of chlordimeform with hydroxyl. The reactions of H-abstraction and addition-dissociation occurring on the side chains are shown in Scheme 1. The reactions of abstraction and addition-dissociation occurring on the benzene ring of chlordimeform are listed in Scheme 2. The corresponding abstraction reaction is denoted as **a**, the addition reaction is denoted as **b**, the dissociation reaction is denoted as **c**, the addition-dissociation reaction is denoted as **bc**, reaction channels are represented to **R**, and products are abbreviated to **P**. The total rate constant of the abstraction reactions and addition reactions occurring on different active sites of benzene ring are $k_{ph\text{-}abs}$ and $k_{ph\text{-}add}$, respectively, $k_{ph\text{-}abs} = k_{3a} + k_{4a} + k_{5a} + k_{6a} + k_{7a}$, $k_{ph\text{-}add} = k_{3b} + k_{4b} + k_{5b} + k_{6b} + k_{7b} + k_{8b}$. While the total rate constant of abstraction reactions and addition reactions on

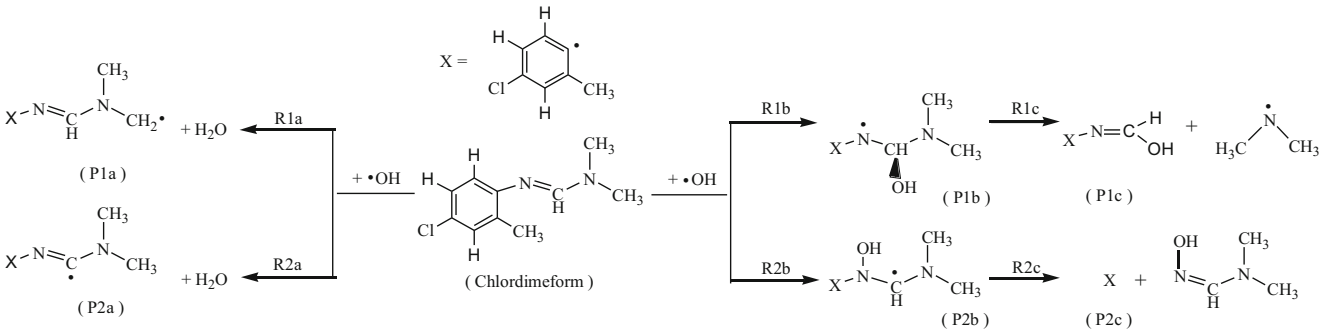

Scheme 1 H- abstraction and addition-dissociation occurring on the side chains of chlordimeform

side chains are $k_{s\text{-}abs}$ and $k_{c=n}$, respectively, $k_{s\text{-}abs}=k_{1a}+k_{2a}$, $k_{c=n}=k_{1b}+k_{2b}$. The total rate constant k is calculated from the sum of the individual rate constants, i.e., $k=k_{ph\text{-}abs}+k_{ph\text{-}add}+k_{s\text{-}abs}+k_{c=n}$.

Kinetic studies on these reactions have been very limited despite their practical and theoretical importance. In 2005, the total rate constant for the gas-phase reaction of the volatile chlordimeform with the hydroxyl was measured, giving a value of $(3.0\pm0.7)\times10^{-10}$ $cm^3molecule^{-1}$ s^{-1} at 296 K using a relative rate method [17]. No experimental information about the branching ratios is available for these reactions. In addition, no experimental information is available on a larger temperature range for the title reactions and the contributions of each possible reaction channel rate to the total rate. To the best of our knowledge, no previous theoretical work has been performed on the kinetics of the title reactions. Theoretical investigation is desirable to further our understanding of the mechanism of these

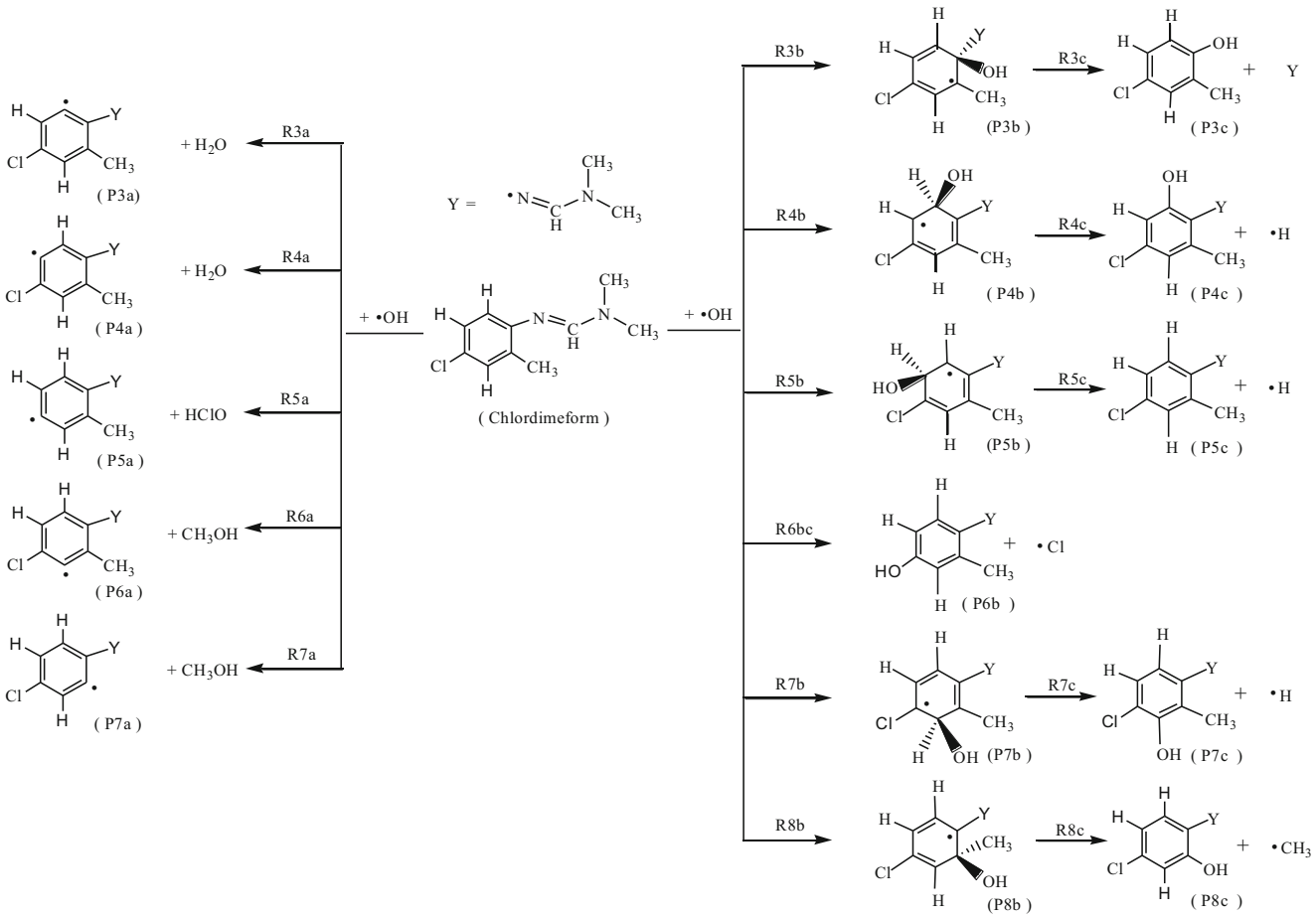

Scheme 2 Abstraction and addition-dissociation occurring on the benzene ring of chlordimeform

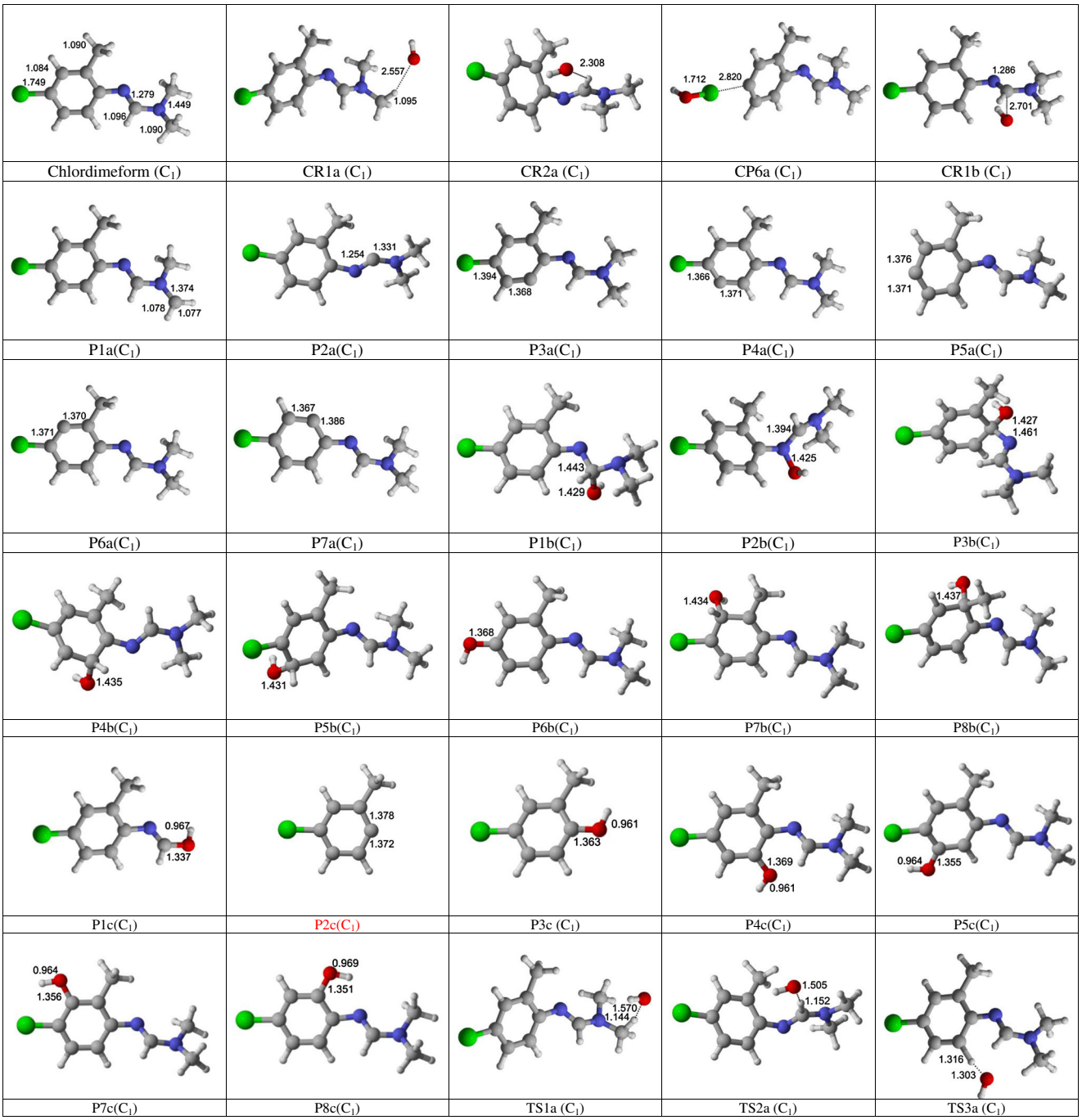

Fig. 1 Optimized geometries of the reactants, complexes, transition states and products at the M06-2X/6-311++G(d,p) level. Bond lengths are in Ångstrom and angles are in degrees

multiple channel reactions and to evaluate the rate constant at high temperatures.

In this paper, a dual-level (X//Y) direct dynamics method [25–29] was employed to study the kinetics of the reactions of chlordimeform with hydroxyl. Potential energy surface information, including geometries, energies, gradients, force constants of all the stationary points (reactants, complexes, transition states, and products) and plus 16 selected points (8 points on each side of saddle point) along the minimum energy path (MEP), was obtained directly from electronic structure calculations. Subsequently, by means of the POLYRATE 9.7 program [30], the rate constants were calculated using variational transition state theory (VTST) [31, 32] as proposed by Truhlar and co-workers. The theoretical and experimental results are compared and

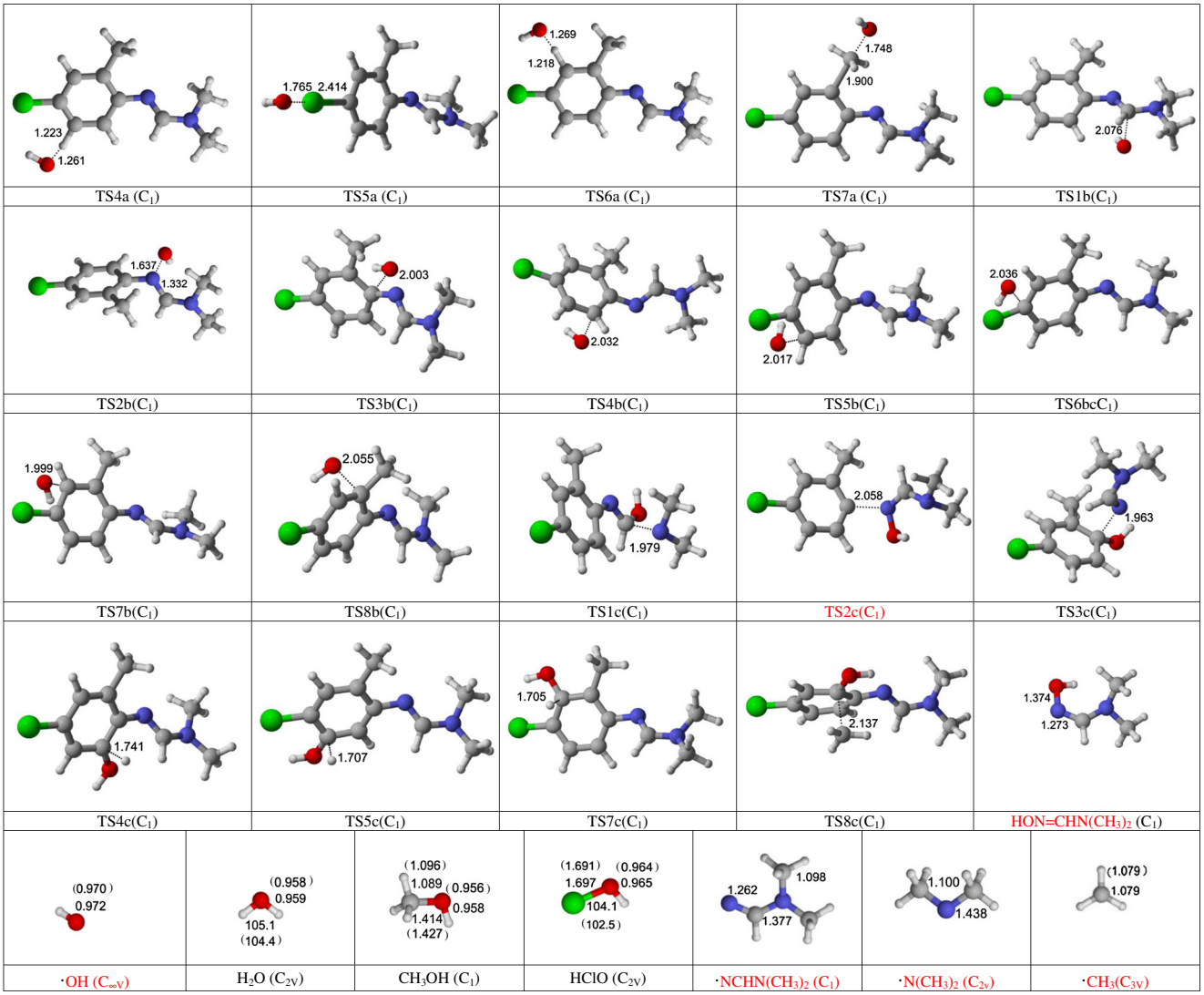

Fig. 1 (continued)

discussed. Our results may be helpful for further experimental investigations.

Computational methods

In the present work, the geometries of the reactants, complexes, transition states and products of the title reaction of chlordimeform with OH radicals were calculated using M06-2X [33] functional with the 6-311++G(d,p) basis set. In order to obtain more accurate energy information of the potential energy surface, the single-point energy of the stable points and the selected points along the MEP were calculated at M06-2X/6-311++G(3df,2p) level based on the geometries optimized at M06-2X/6-311++G(d,p) level. All the electronic structure calculations were performed using the GAUSSIAN09 program package [34]. In addition, we calculated the rate constant of the reaction of chlordimeform with OH radicals using improved canonical variational transition state theory (ICVT) [35–37] with the small-curvature tunneling (SCT) [38, 39] correction by means of the POLYRATE 9.7 program [30]. All vibrational modes are treated as quantum-mechanical separable harmonic oscillators, except for the lowest vibrational modes of the transition states, which are treated by the hindered rotor model [40, 41] to be used for calculating the partition function. In the calculation of the reactant electronic partition function, two electronic states of OH radicals were included, with a 140 cm^{-1} splitting due to spin-orbit coupling. During the kinetic calculations, the Euler single-step integrator with a step size of 0.0001 $(amu)^{1/2}$ bohr was used to follow the MEP, and generalized normal-mode analysis was performed every 0.01 $(amu)^{1/2}$ bohr. The curvature

Table 1 The reaction enthalpies at 298 K (ΔH^0_{298}), the potential barrier heights (ΔE^{TS}) (kcal mol^{-1}) with zero-point energy (ZPE) correction for the reactions of chlordimeform with OH radicals at the M06-2X/6-311++G(3df,2p)//M06-2X/6-311++G(d,p) level

	ΔH^0_{298}	ΔE^{TS}+ZPE
R1a	−25.86	−0.70
R2a	−18.59	−2.21
R3a	−6.24	11.18
R4a	−4.77	4.83
R5a	41.55	39.15
R6a	−4.94	2.62
R7a	11.04	45.24
R1b	−29.58	−2.38
R2b	9.73	13.16
R3b	−19.18	2.17
R4b	−18.36	3.07
R5b	−20.33	0.84
R6bc	−13.45	4.25
R7b	−19.22	0.84
R8b	−22.38	0.08
R1c	−14.96	−6.27
R2c	42.98	49.84
R3c	−14.16	−6.09
R4c	0.16	6.33
R5c	−2.83	5.27
R7c	−2.83	4.70
R8c	−13.52	−1.25

components were calculated by using a quadratic fit to obtain the derivative of the gradient with respect to the reaction coordinate.

Results and discussion

Stationary points

The equilibrium geometries of the reactants, complexes, products, and transition states obtained at the M06-2X/6-311++G(d,p) level are presented in Fig. 1. It can be seen that the theoretical geometric parameters at the M06-2X/6-311++G(d,p) level of the species OH, H_2O, CH_3, HClO, and CH_3OH are in good agreement with the corresponding available experimental values [42, 43]. The reactant complexes (CR1a, CR2a, and CR1b) are formed in the entrance of channel R1a, R2a, and R1b; the product complexes CP6a are formed in the exit of channel R6a. At the M06-2X/6-311++G(d,p) level, the O···H bond distances in CR1a and CR2a are 2.557 and 2.308 Å, respectively, the O···C bond distance in CR1b is 2.701 Å, while the other bond lengths are very close to those of the corresponding reactants; the O···Cl bond distance in CP6a is 1.712 Å, while the other bond lengths are very close to those of the corresponding product. In the structures of TS1a, TS2a, TS3a, TS4a, and TS6a, the breaking bonds C—H are increased by 4.28, 5.11, 7.14, 12.36, 12.93, and 25.74 % compared to the equilibrium bond length in chlordimeform; and the forming O—H bonds are stretched by 63.71, 56.93, 49.22, 32.33, 31.49, and 29.77 % over the equilibrium bond lengths in isolated H_2O, respectively. The elongation of the breaking bonds is less than that of the forming bonds, indicating that TS1a, TS2a, TS3a, TS4a, and TS6a of the title reaction systems are all reactant-like, i.e., the seven reaction channels will proceed via "early" transition states, which is consistent with Hammond's postulate [44] for exothermic reactions. In TS5a and TS7a structures, the breaking bonds C—H are increased by 38.02 and 26.41 % comparing with the equilibrium bond length in chlordimeform; and the forming bonds O—H are stretched by 4.01 % and 23.62 % over the equilibrium bond lengths in isolated H_2O, respectively. The elongation of the breaking bond is larger than that of the forming bond, indicating that R5a and R7a of the title reaction systems are all reactant-like, i.e., the two reaction channels will proceed via "late" transition states, according to Hammond's postulate [44] for an endothermic reaction.

The harmonic vibrational frequencies of the reactants, complexes, products, and transition states calculated at the M06-2X /6-311++G(d,p) level are listed in Table S1 as supplementary information, as well as the available experimental values [45, 46]. For the species OH, H_2O and CH_3OH, the calculated frequencies are in good agreement with experimental values, with the largest deviation being 6 %. The 23 transition states were all confirmed by normal-mode analysis to have one, and only one, imaginary frequency, which corresponds to stretching mode coupling between breaking and forming bonds.

Energetics

The reaction enthalpies (ΔH^0_{298}) and potential barrier heights (ΔE^{TS}) with zero-point energy (ZPE) corrections for reaction of chlordimeform with OH radicals calculated at the M06-2X/6-311++G(3df,2p)//M06-2X /6-311++G(d,p) level are listed in Table 1. A schematic potential energy surface of abstraction reaction channel of chlordimeform with OH radicals is plotted in Fig. 2, and schematic potential energy surface addition-dissociation reaction channel of chlordimeform with OH radicals at M06-2X/6-311++G(3df,2p)//M06-2X/6-311++G(d,p) level is plotted in Fig. 3, including ZPE corrections. For ease of discussion, the energy of the reactant was set to zero for reference. From Table 1, it can be seen that the abstraction reactions R1a-4a and R6a are all exothermic reactions, and R5a and R7a are endothermic reactions, which is consistent with the discussion of Hammond's postulate [44]. Calculations show that the addition reaction R1b is a barrierless association, the attack of OH radicals on the C–N bond would

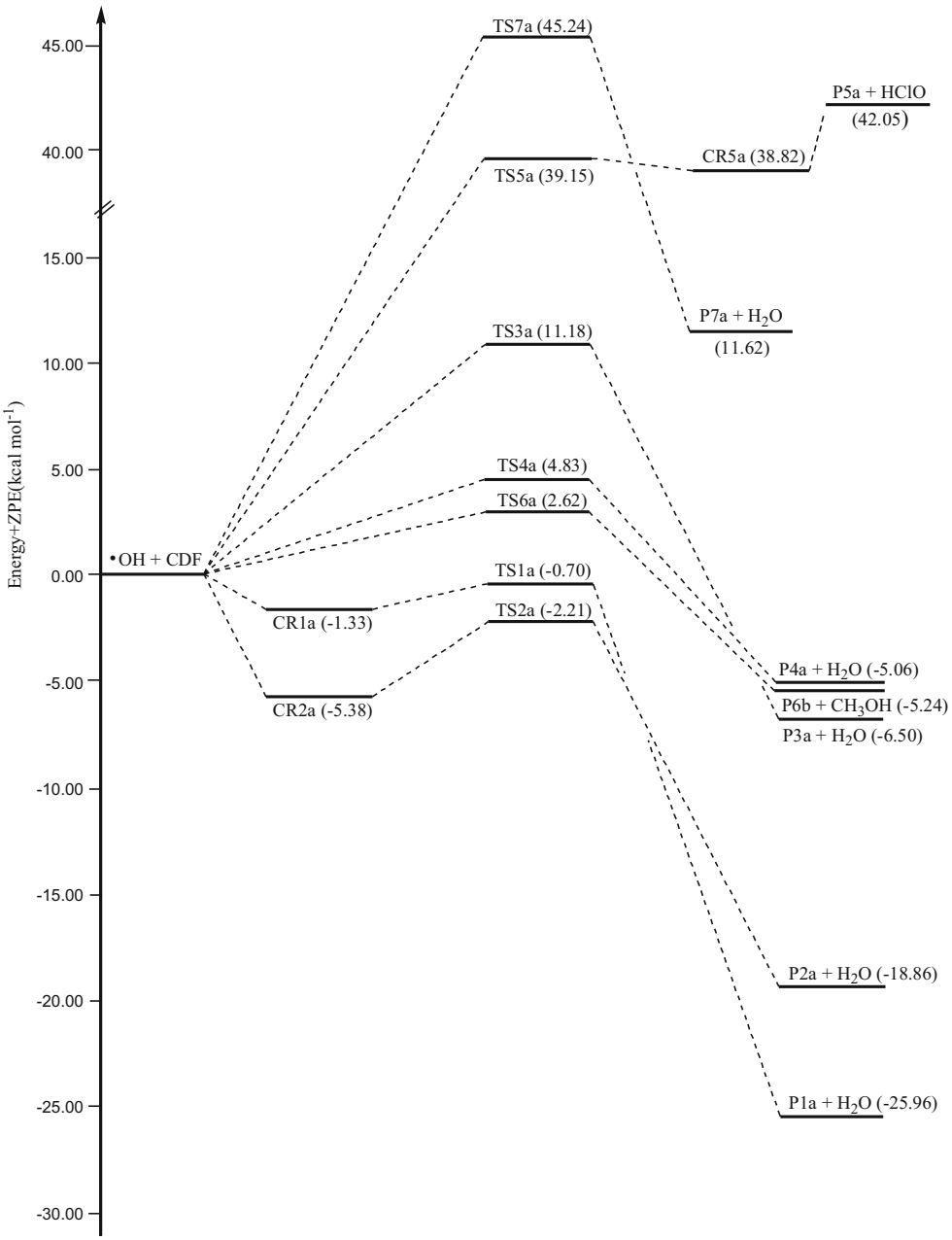

Fig. 2 Schematic potential energy surface (PES) of abstraction reaction channel of the title reaction system. Relative energies are calculated at the M06-2X/6-311++G(3df,2p)// M06-2X/6-311++G(d,p) + ZPE level (in kcal mol^{-1})

proceed via a complex (CR1b), which is about 6.19 kcal mol^{-1} lower than that of the corresponding reactants. And reaction R1b is more exothermic than reactions R1a, R2a, R3a, R4a, R5a, R6a, R7a, R2b, R3b, R4b, R5b, R6bc, R7b, and R8b by 3.72, 10.99, 23.34, 24.81, 71.13, 24.64, 40.62, 39.31, 10.40, 11.22, 9.25, 16.13, 10.36, and 7.20 kcal mol^{-1}, respectively. Therefore, the reaction channel R1b is the major reaction channel.

From Table 1, it can be seen that the addition reaction has more advantage than the corresponding abstraction reaction for every active site on the benzene ring. Also, the energy barrier height of addition channel R8b is lower than that of other addition channels (R3b–R7b), the channel R8b is the most active addition channel, but the energy barrier height of abstraction channel R7a—the corresponding site on benzene ring to the addition channel R8b—is higher than that of other abstraction channels (R3a–R6a), therefore channel R7a is the most inactive abstraction channel.

Rate constants

Dual-level dynamics calculations of the title reaction are carried out at the M06-2X/6-311++G(3df,2p)// M06-2X/6-311++G(d,p) level. The rate constants of the individual channel are evaluated by improved canonical variational transition

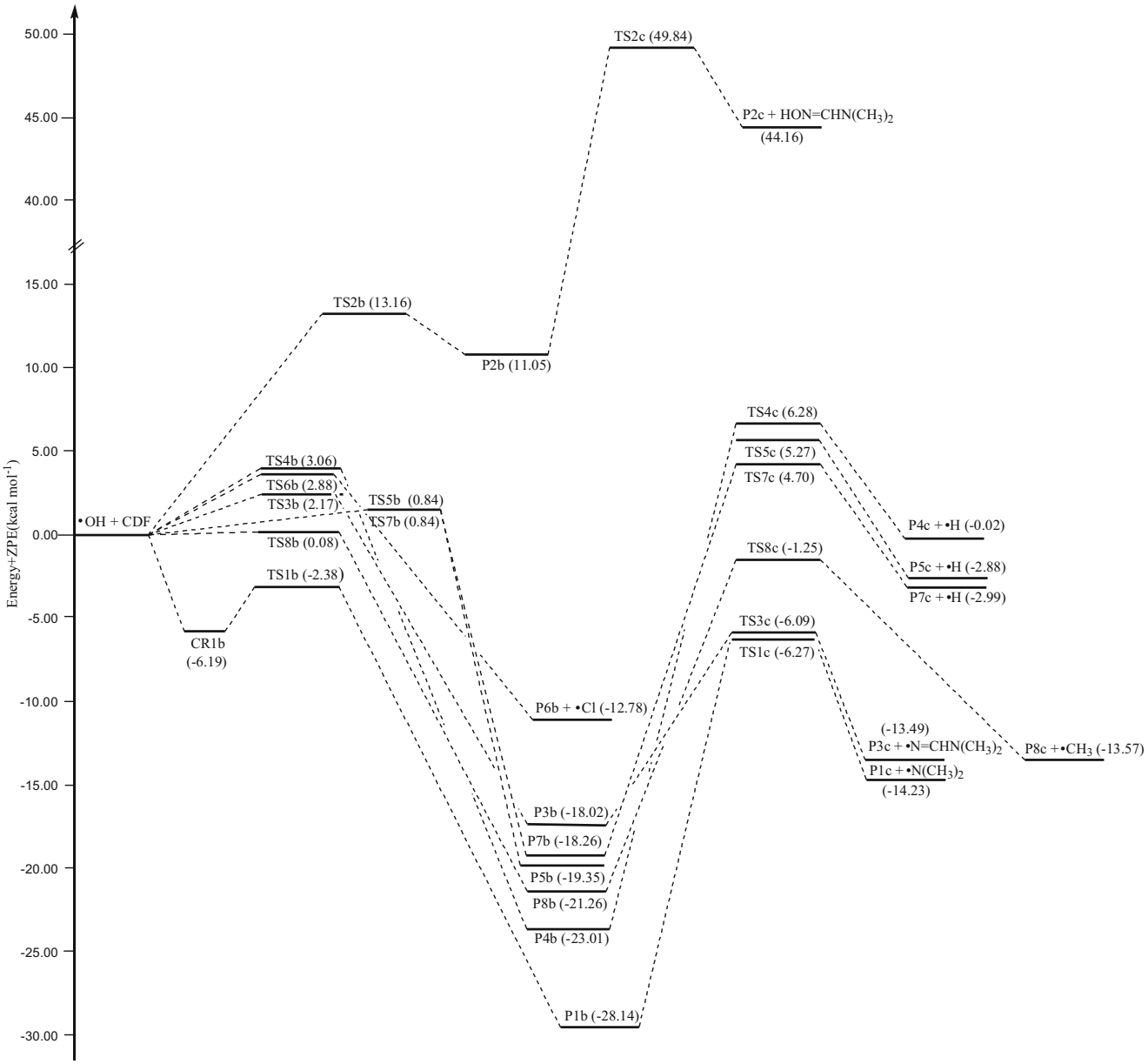

Fig. 3 Schematic PES of addition-dissociation reaction channel of the title reaction system. Relative energies are calculated at the M06-2X/6-311++G(3df,2p)// M06-2X/6-311++G(d,p)+ZPE level (in kcal mol^{-1})

(ICVT) state theory in a wide temperature range from 200 to 1,000 K. The ICVT/SCT rate constants of abstraction reaction and addition reaction channels are listed in Table S2 and Table S3, and the ICVT/SCT rate constants for $k_{ph\text{-}abs}$, $k_{ph\text{-}add}$, $k_{s\text{-}abs}$, $k_{c=n}$, and k are listed in Table 2. The ICVT/SCT rate constants of the major channels are plotted against the reciprocal of temperature in Fig. 4 along with the available experimental results [17]. The measured value in [17] is the consumption of reactant, so we discuss here only the first step reaction process, in which the consumption of the reactant chlordimeform occurred. Steps 1c–8c are the follow-up reaction, i.e., not included in the consumption of the reactant, so are not discussed in detail, and the rate constants of 1c–8c were not included in expressions for effective rate constants. From Fig. 4, it can be seen that the addition reactions of the carbon=nitrogen double bond are the major reaction channels over the temperature range 200–1,000 K. This is consistent with the above-mentioned corresponding potential energy barrier heights. The calculated total rate constant value of k at 296 K, 2.80×10^{-10} cm^{3}molecule^{-1} s^{-1}, is in good agreement with the available experimental value [17], $(3.0\pm0.7)\times10^{-10}$ cm^{3}molecule^{-1} s^{-1}, and the ratio of k_{exptl} / $k_{ICVT/SCT}$ is 0.93.

To further understand the reaction mechanism of the title reaction and the temperature dependence of branching ratios, the calculated branching ratios are exhibited against the reciprocal of temperature in Fig. 5. As can be seen, the addition

Table 2 Calculated improved canonical variational transition/small-curvature tunneling (ICVT/SCT) rate constants (cm^3 $molecule^{-1}$ s^{-1}) for $k_{ph\text{-}abs}$, $k_{ph\text{-}add}$, $k_{s\text{-}abs}$, $k_{c=n}$, and k in the temperature range 200–1,000 K at the M06-2X/6-311++G(3df,2p)//M06-2X/6-311++G(d,p) level together with the corresponding experimental values

T(K)	$k_{s\text{-}abs}$ ICVT/SCT	$k_{ph\text{-}abs}$ ICVT/SCT	$k_{c=n}$ ICVT/SCT	$k_{ph\text{-}add}$, ICVT/SCT	k ICVT/SCT	$k_{reference}$
200	1.85×10^{-10}	3.97×10^{-14}	2.37×10^{-10}	3.43×10^{-13}	4.22×10^{-10}	
225	1.18×10^{-10}	6.11×10^{-14}	2.23×10^{-10}	5.87×10^{-13}	3.42×10^{-10}	
250	8.89×10^{-11}	8.94×10^{-14}	2.15×10^{-10}	9.04×10^{-13}	3.05×10^{-10}	
296	6.84×10^{-11}	1.62×10^{-13}	2.10×10^{-10}	1.69×10^{-12}	2.80×10^{-10}	$(3.0\pm0.7)\times10^{-10}$
350	6.18×10^{-11}	2.88×10^{-13}	2.14×10^{-10}	2.99×10^{-12}	2.79×10^{-10}	
400	6.13×10^{-11}	4.53×10^{-13}	2.25×10^{-10}	4.60×10^{-12}	2.91×10^{-10}	
450	6.34×10^{-11}	6.72×10^{-13}	2.40×10^{-10}	6.66×10^{-12}	3.11×10^{-10}	
500	6.71×10^{-11}	9.56×10^{-13}	2.59×10^{-10}	9.24×10^{-12}	3.36×10^{-10}	
600	7.81×10^{-11}	1.76×10^{-12}	3.09×10^{-10}	1.62×10^{-11}	4.05×10^{-10}	
700	9.32×10^{-11}	2.98×10^{-12}	3.74×10^{-10}	2.65×10^{-11}	4.97×10^{-10}	
800	1.12×10^{-10}	4.71×10^{-12}	4.52×10^{-10}	4.02×10^{-11}	6.09×10^{-10}	
900	1.34×10^{-10}	7.11×10^{-12}	5.46×10^{-10}	5.81×10^{-11}	7.45×10^{-10}	
1,000	1.61×10^{-10}	1.03×10^{-11}	6.54×10^{-10}	8.13×10^{-11}	9.07×10^{-10}	

reactions of the carbon=nitrogen double bond dominate the reaction over the whole temperature region. And the electronegativity of the N atom in the carbon=nitrogen double bond is stronger than that of the C atom, facilitating attack of the latter by the OH radical through an addition mechanism. This is consistent with the analysis of above-mentioned potential energy barrier heights.

Because investigation of the temperature region of the rate constant is always limited in experimental studies, we hope that our kinetics research may provide useful information for laboratory investigations in the future. In order to provide more convenient reference data, a three-parameter fitting of the ICVT/SCT rate constants for the 15 reaction channels and the total rate constants performed over the temperature range 200–1,000 K are given as follows (in $cm^3molecule^{-1}$ s^{-1}):

$$k_{1a}(T) = 1.20 \times 10^{-17} T^{2.27} \exp(722.65/T)$$

$$k_{2a}(T) = 1.29 \times 10^{-19} T^{2.05} \exp(1969.02/T)$$

$$k_{3a}(T) = 2.47 \times 10^{-23} T^{3.08} \exp(-284.47/T)$$

$$k_{4a}(T) = 2.60 \times 10^{-22} T^{3.03} \exp(324.70/T)$$

$$k_{5a}(T) = 1.55 \times 10^{-18} T^{2.10} \exp(-2323.25/T)$$

$$k_{6a}(T) = 6.63 \times 10^{-21} T^{3.08} \exp(-205.69/T)$$

$$k_{7a}(T) = 4.37 \times 10^{-21} T^{2.28} \exp(-3384.43/T)$$

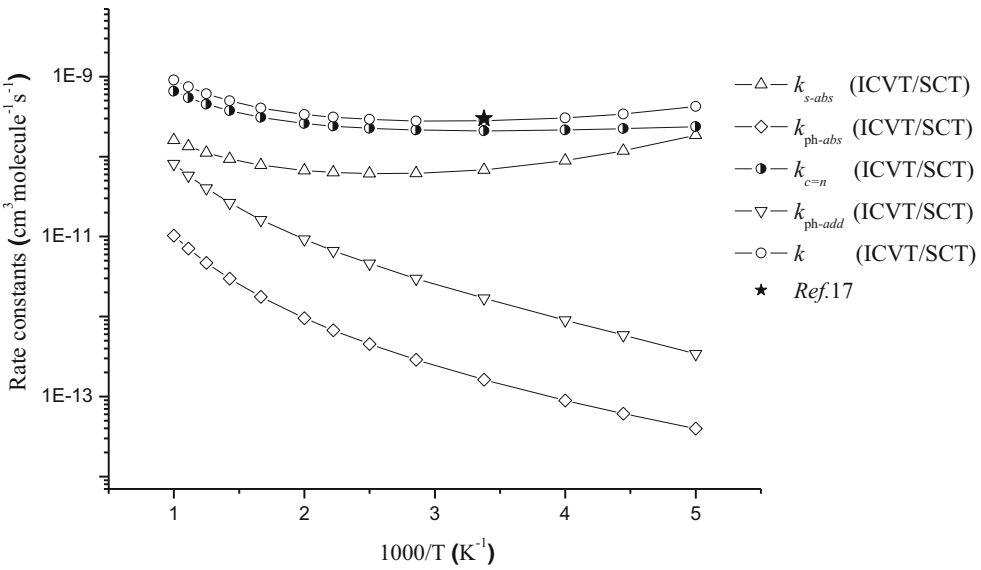

Fig. 4 Calculated improved canonical variational transition/small-curvature tunneling (ICVT/SCT) rate constants for major channels and total rate constants k (in $cm^3molecule^{-1}$ s^{-1}) versus 1,000/T between 200 and 800 K at the M06-2X/6-311++G(3df,2p)//M06-2X/6-311++G(d,p) level, together with the available experimental values

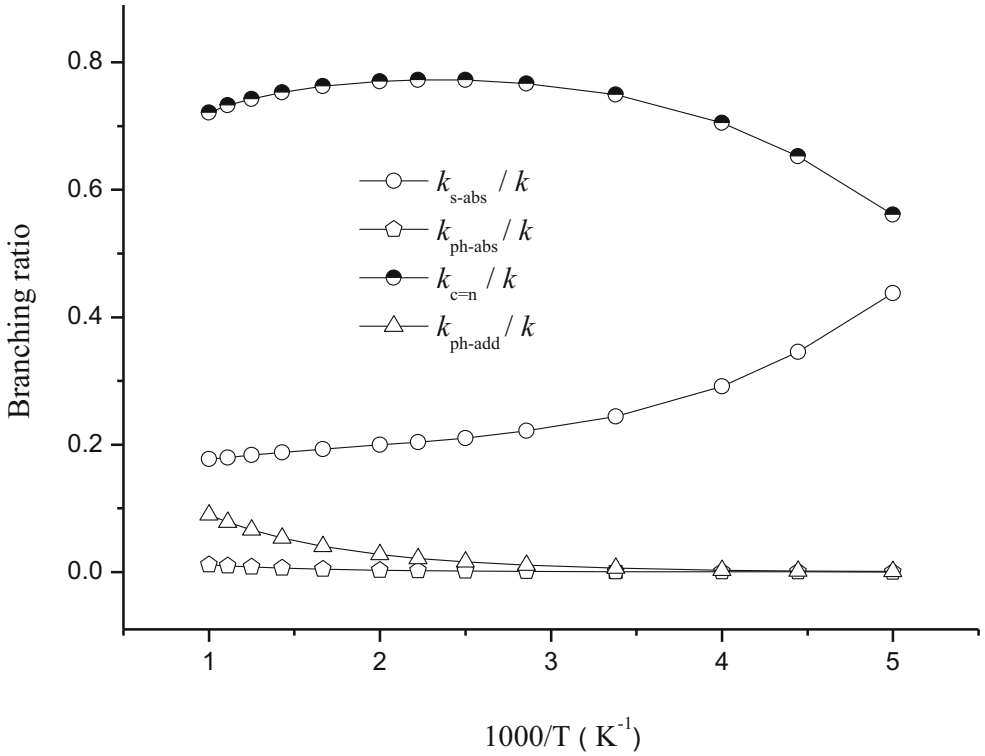

Fig. 5 Calculated branching ratios for the title reaction versus 1,000/T between 200 and 1,000 K. See Fig. 1

$$k_{1b}(T) = 8.76 \times 10^{-17} T^{2.19} \exp(645.22/T)$$

$$k_{2b}(T) = 3.38 \times 10^{-21} T^{2.11} \exp(-973.24/T)$$

$$k_{3b}(T) = 1.06 \times 10^{-17} T^{1.99} \exp(-463.24/T)$$

$$k_{4b}(T) = 1.49 \times 10^{-19} T^{2.69} \exp(-551.50/T)$$

$$k_{5b}(T) = 1.38 \times 10^{-24} T^{4.40} \exp(240.78/T)$$

$$k_{6b}(T) = 1.20 \times 10^{-19} T^{2.66} \exp(-499.88/T)$$

$$k_{7b}(T) = 6.61 \times 10^{-19} T^{2.59} \exp(-529.32/T)$$

$$k_{8b}(T) = 2.12 \times 10^{-16} T^{1.61} \exp(-330.38T)$$

$$k(T) = 2.62 \times 10^{-18} T^{2.71} \exp(899.61/T)$$

Conclusions

In this work, the multi-channel reactions of chlordimeform with OH radicals were investigated theoretically by means of direct dynamics methods. Optimized geometries and harmonic vibrational frequencies of the stationary points at the M06-2X/6-311++G(d,p) level were in good agreement with the corresponding experimental values. The theoretic identification of 15 feasible reaction channels is completed at M06-2X/6-311++G(3df,2p)//M06-2X/6-311++G(d, p) level, which infers that the main reaction includes concerted abstraction, addition-dissociation and addition-dissociation reactions. An evaluation of each reaction channel focusing on the consumption rate of reactants was also expounded. Meanwhile, the theoretical results showed that the reaction rate of chlordimeform with OH is of the order of magnitude of 10^{-10} $cm^3 molecule^{-1}$ s^{-1} , meaning that OH radicals can promote the degradation of chlordimeform in atmosphere.

Acknowledgments The authors thank Professor Donald G. Truhlar for providing the POLYRATE 9.7 program. This work was supported by the National Basic Research Program of China (2012CB723308), the National Natural Science Foundation of China (51337002 and 50977019), the Doctoral Foundation by the Ministry of Education of China (20112303110005), and the Science Foundation for Distinguished Young Scholar of Heilongjiang Province (JC201206).

References

1. Serra-Bonvehí J, Orantes-Bermejo J (2010) Pest Manag Sci 66:1230

2. Shi J, Chen GH, Tong MZ, Wu X, Wang K (2011) J Hebei Univ Sci Technol 32:421
3. Sun TF (2010) J Anhui Agric Sci 38:11981
4. Zhou ZQ, Ding HY, Jiang XY, Wu J (2009) Agrochemicals Res Appl 13:27
5. Yu JL (2009) J Shandong Inst Commer Technol 9:123
6. Fang R, Yi LX, Shao YX, Zhang L, Chen GH (2013) J Liq Chromatogr R T 20:79740
7. Li W, Sun M, Li MZ (2013) Adv J Food Sci Technol 5:381
8. Chamkasem N, Ollis LW, Harmon T, Lee S, Mercer G (2013) J Agric Food Chem 61:2315
9. Watkinson WPJ (1986) Toxicol Environ Health 19:207
10. Lund AE, Yim GKW, Shankland DL (1978) Pesticide Venom Neurotoxicity 46:171
11. Lund AE, Shankland DL, Chinn C, Yim GKW (1978) Toxicol Appl Pharmacol 44:357
12. Popp W, Schmieding W, Speck M, Vahrenholz C, Norpoth K (1992) Br J Ind Med 49:529
13. Kirkali Z, Chan T, Manoharan M, Algaba F, Busch C (2005) Urology 66:4
14. Vineis P (1994) Environ Health Perspect 102:7
15. Vineis P, Pirastu R (1997) Cancer Cause Control 8:346
16. Rapiti E, Fantini F, Dell'Orco V, Fano V (1997) Eur J Epidemiol 13:281
17. Sun F, Zhu T, Shang J, Han L (2005) Int J Chem Kinet 37:755
18. Jimenez JJ, Bernal JL, Toribio LJ (2002) Chromatogr A 946:247
19. Corta E, Bakkali A, Barranco A, Berrueta LA, Gallo B (2000)Talanta 52:169
20. Hamed MS, Knowles CO (1988) J Econ Entomol 81:1295
21. Knowles CO, Benezet HJJ (1977) Agric Food Chem 25:022
22. Lee W, Stevens PS, Hites RA (2003) J Phys Chem A 107:6603
23. Crutzen PJ, Ramanathan V (2000) Science 290:299
24. Atkinson R (1988) In: Watson AY, Bates RR, Kennedy D(eds) Air pollution, the automobile, and public health. National Academy Press, Washington, DC, p 99
25. Corchado JC, Espinosa-Garcia J, Hu WP, Rossi I, Truhlar DG (1995) J Phys Chem 99:687
26. Hu WP, Truhlar DG (1996) J Am Chem Soc 118:860
27. Bell RL, Truong TN (1994) J Chem Phys 101:10442
28. Truong TN, Duncan WT, Bell RL (1996) In: Laird BB, Ross RB, Ziegler T (eds) Chemical applications of density functional theory. American Chemical Society, Washington, DC, p 85
29. Truhlar DG (1995) In: Heidrich D (ed) The reaction path in chemistry: current approaches and perspectives. Kluwer, Dordrecht, p 229
30. Corchado JC, Chuang YY, Fast PL, Hu WP, Liu YP, Lynch GC, Nguyen KA, Jackels CF, Fernandez-Ramos A, Ellingson BA, Lynch BJ, Zheng JJ, Melissasa VS,Villa J, Rossi I, Coitino EL, Pu JZ, Albu TV, Steckler R, Garrett BC, Isaacson AD, Truhlar, DG (2007) POLYRATE version 9.7, Department of Chemistry and Supercomputer Institute, University of Minnesota, Minneapolis
31. Truhlar DG, Garrett BC (1980) Accounts Chem Res 13:440
32. Truhlar DG, Isaacson AD, Garrett BC (1985) In: Baer M (ed) Generalized transition state theory: in the theory of chemical reaction dynamics, vol 4. CRC, Boca Raton, p 65
33. Zhao Y, Truhlar DG (2008) Theor Chem Acc 120:215
34. Frisch MJ, Trucks GW, Schlegel HB, Scuseria GE, Robb MA, Cheeseman JR, Scalmani G, Barone V, Mennucci B, Petersson GA, Nakatsuji H, Caricato M, Hratchian XLiHP, Izmaylov AF, Bloino J, Zheng G, Sonnenberg JL, Hada M, Ehara M, Toyota K, Fukuda R, Hasegawa J, Ishida M, Nakajima T, Honda Y, Kitao O, Nakai H, Vreven T, Montgomery JA, Peralta JrJE, Ogliaro F, Bearpark M, Heyd JJ, Brothers E, Kudin KN, Staroverov VN, Kobayashi R, Normand J, Raghavachari K, Rendell A, Burant JC, Iyengar SS, Tomasi J, Cossi M, Rega N, Millam JM, Klene MJ, Knox EJ, Cross B, Bakken V, Adamo C, Jaramillo J, Gomperts R, Stratmann RE, Yazyev O, Austin AJ, Cammi R, Pomelli C, Ochterski JW, Martin RL, Morokuma K, Zakrzewski VG, Voth GA, Salvador PJ, Dannenberg J, Dapprich S, Daniels AD, Farkas O, Foresman JB, Ortiz JV, Cioslowski J, Fox DJ (2009) Gaussian, Inc., Revision A.02, Wallingford CT
35. Baldridge MS, Gordor R, Steckler R, Truhlar DG (1989) J Phys Chem 93:5107
36. Gonzalez-Lafont A, Truong TN, Truhlar DG (1991) J Chem Phys 95: 8875
37. Garrett BC, Truhlar DG (1979) J Phys Chem 83:1052
38. Lu DH, Truong TN, Melissas VS, Lynch GC, Liu YP, Grarrett BC, Steckler R, Issacson AD, Rai SN, Hancock GC, Lauderdale JG, Joseph T, Truhlar DG (1992) Comput Phys Commun 71:235
39. Liu YP, Lynch GC, Truong TN, Lu DH, Truhlar DG, Garrett BC (1993) J Am Chem Soc 115:2408
40. Truhlar DG (1991) J Comput Chem 12:266
41. Chuang YY, Truhlar DG (2000) J Chem Phys 112:1221
42. Huber KP, Herzberg G (2005) In NIST Chemistry WebBook; NIST Standard Reference Database Number 69
43. Kuchitsu K (ed) (1998) Structure of free polyatomic molecules basic data. Springer, Berlin, p 58
44. Hammond GS (1955) J Am Chem Soc 77:334
45. Shimanouchi T (1972) In: Tables of molecular vibrational frequencies consolidated volume I, National Bureau of Standards, US GPO: Washinton DC
46. Coblentz Society (2005) In NIST Chemistry WebBook; NIST Standard Reference Database Number 69